

Accepted Manuscript

3D supramolecular networks based on hydroxyl-rich Schiff-base copper(II) complexes

Katerina N. Lazarou, Aikaterini Savvidou, Catherine P. Raptopoulou, Vassilis Psycharis

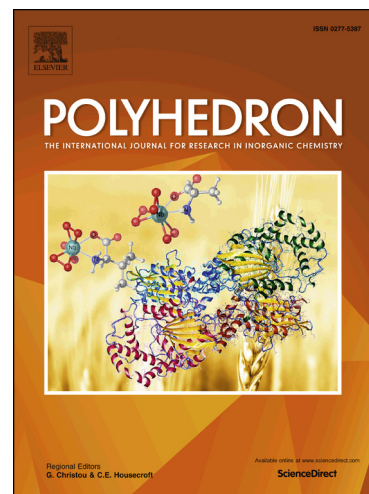
PII: S0277-5387(18)30317-6
DOI: <https://doi.org/10.1016/j.poly.2018.06.001>
Reference: POLY 13208

To appear in: *Polyhedron*

Received Date: 19 April 2018

Please cite this article as: K.N. Lazarou, A. Savvidou, C.P. Raptopoulou, V. Psycharis, 3D supramolecular networks based on hydroxyl-rich Schiff-base copper(II) complexes, *Polyhedron* (2018), doi: <https://doi.org/10.1016/j.poly.2018.06.001>

This is a PDF file of an unedited manuscript that has been accepted for publication. As a service to our customers we are providing this early version of the manuscript. The manuscript will undergo copyediting, typesetting, and review of the resulting proof before it is published in its final form. Please note that during the production process errors may be discovered which could affect the content, and all legal disclaimers that apply to the journal pertain.



**3D supramolecular networks based on hydroxyl-rich Schiff-base
copper(II) complexes†**

Katerina N. Lazarou, Aikaterini Savvidou, Catherine P. Raptopoulou* and Vassilis Psycharis*

*Institute of Nanoscience and Nanotechnology, NCSR “Demokritos”, 15310 Aghia Paraskevi,
Athens, Greece*

† This work is dedicated to our dearest friend and colleague Prof. Spyros P. Perlepes on the occasion of his 65th birthday and in recognition of his enormous contribution to the development of Inorganic Chemistry.

*Corresponding author: Tel: +30 210 6503346; Fax: +30 210 6519430

E-mail address: c.raptopoulou@inn.demokritos.gr (Dr. C.P.Raptopoulou)

E-mail address: v.psycharis@inn.demokritos.gr (Dr. V. Psycharis)

Abstract

Reactions of the Schiff base ligand OH-C₆H₄-CH=NC(CH₂OH)₃ (H₄L) with copper(II) salts in various reaction media afforded complexes [Cu₄(H₂L)₄]·MeOH (**1**·MeOH), [Cu₂(O₂CMe)₂(H₃L)₂] (**2**), [Cu₄(H₂L)₄(H₂O)₂]·1.5dmf (**3**·1.5dmf), [Cu₄(H₂L)₄(H₂O)]·MeOH (**4**·MeOH) and [Cu₄(H₂L)₄]₂·2H₂O·7MeOH (**5**·2H₂O·7MeOH). Compounds **1**, **3** and **4** consist of neutral tetranuclear entities in which the Cu^{II} ions are coordinated by the tridentate Schiff base ligands, forming a tetranuclear Cu₄O₄ cubane-like configuration. Compound **5** contains similar cubane-like tetranuclear entities which are further linked through the hydroxyl groups of the ligands thus forming dimers of cubanes. Compound **2** contains a neutral dinuclear entity in which the Cu^{II} ions are bridged through the Schiff base and the acetate ligands, comprising distorted Cu₂O₂ core. The Schiff base ligand adopts five different coordination modes and two deprotonation states in the structures of **1-5** acting simultaneously as chelating and bridging agent between the metal ions. The lattice structures of **1-5** exhibit interesting 3D networks based on hydrogen bonded metal clusters and they are studied with Hirshfeld Surface analysis methods.

Keywords: copper(II) complexes, cubane structures, Schiff base ligands, crystal structures, supramolecular networks, Hirshfeld surface analysis

1. Introduction

Porous coordination polymers, widely known as metal-organic frameworks (MOFs), have been the major subject of materials chemistry during the last decades. In many cases, these materials exhibit intricate and beautiful crystal structures. The main feature of MOFs is the porosity which makes them the organic-inorganic hybrid analogs of zeolites and therefore have found several applications such as storage and separation of gases, drug delivery, catalysis, and functional materials (e.g. sensors, luminescent and magnetic materials) [1-3]. The formation of MOFs is based on the covalent interactions between the metal ions and the donor atoms of the ligands. However, the presence of noncovalent interactions, such as hydrogen bonding and π - π interactions are very important for the stability of MOFs, and most importantly for the formation of supramolecular networks based on organic and/or hybrid organic-inorganic building units. Noncovalent interactions control vital biological processes in living systems with the most important ones being the proteins' structure and functionality. Supramolecular networks based on various nuclearity metal complexes have been the major subject of crystal engineering and have been extensively studied. The building blocks of these networks are held together via noncovalent interactions with the most important being hydrogen bonds, although other type of interactions such as halogen, chalcogen and pnictogen interactions have gained attention recently. Supramolecular metal networks based on n - π^* , π - π stacking, π -cation, π -anion and hydrophobic interactions have been also reported [4-6]. Such materials have been examined for potential applications in separation technology and catalysis based on host-guest chemistry principles [7-9].

Schiff bases can be easily prepared by reaction of amines with aldehydes or ketones [10,11]. The major advantage of this class of organic molecules is the large number of ligands that can be prepared by choosing various starting materials with the desired functional sidegroups. Therefore, Schiff base ligands have been extensively used for the synthesis of 3d, 3d/4f and 4f complexes in order to study their physical properties [12-17] and in many cases exhibit catalytic and significant biological activity [18,19].

One of our research projects aims in the use of Schiff base ligands, that contain simultaneously chelating and bridging groups, in 3d and 3d/4f chemistry. Salicylaldehyde, among other aldehydes, and polyalcohol amines, such as tris(hydroxymethyl)aminomethane, are used to prepare ligand H_4L used in the present study. H_4L has been widely used in transition metal chemistry [20-28]. Our recent results in Schiff bases chemistry involve tetranuclear Mn^{III} complexes with zig-zag chain structure, trinuclear and octanuclear Fe^{III} complexes, as well as heptanuclear heterometallic Cu^{II}/Ln^{III} complexes [29-31]. We present herein the synthesis, spectroscopic and crystallographic characterization of Cu^{II} complexes with H_4L , i.e. the tetranuclear complexes with cubane structure $[Cu_4(H_2L)_4] \cdot MeOH$ (**1**·MeOH), $[Cu_4(H_2L)_4(H_2O)_2] \cdot 1.5dmf$ (**3**·1.5dmf) and $[Cu_4(H_2L)_4(H_2O)] \cdot MeOH$ (**4**·MeOH), the dinuclear complex $[Cu_2(O_2CMe)_2(H_3L)_2]$ (**2**), and the dimer of cubanes complex $[Cu_4(H_2L)_4]_2 \cdot 2H_2O \cdot 7MeOH$ (**5**·2H₂O·7MeOH). We discuss in detail the supramolecular networks formed from **1-5** due to noncovalent interactions by using Hirshfeld surface analysis method.

2. Experimental

2.1. General and spectroscopic measurements

All manipulations were performed under aerobic conditions using materials as received (Aldrich Co). All chemicals and solvents were of reagent grade. Elemental analysis for carbon, hydrogen, and nitrogen was performed on a Perkin Elmer 2400/II automatic analyzer. Infrared spectra were recorded as KBr pellets in the range 4000 - 400 cm^{-1} on a Bruker Equinox 55/S FT-IR spectrophotometer.

2.2. Compound preparations

2.2.1. $OH-C_6H_4-CH=NC(CH_2OH)_3$, H_4L .

Solid tris(hydroxymethyl)aminomethane (10 mmol, 1.210 g) was dissolved in MeOH (15 mL) to afford a colorless solution. A colorless solution of salicylaldehyde (10 mmol, 1.053 mL) in

MeOH (15 mL) was then added to afford a final yellow solution which was stirred at ~ 45 °C for one hour. The final solution was evaporated to dryness under vacuum to yield a yellow product which was extracted by *n*-hexane (5 mL). The final yellow precipitate was dried under vacuum overnight. (Yield: 2.18 g, 96.9 %). $C_{11}H_{15}NO_4$ requires: C, 58.66; H, 6.71; N, 6.22 %. Found: C, 58.42; H, 6.67; N, 6.19 %. FT-IR (KBr pellets, cm^{-1}): 3320(br,s), 3062(w), 3029(w), 2978(m), 2936(m), 2885(m), 2820(m), 1637(vs), 1608(s), 1556(s), 1535(s), 1514(m), 1487(vs), 1456(s), 1424(m), 1395(s), 1382(m), 1366(m), 1340(s), 1306(s), 1279(m), 1225(s), 1189(s), 1153(s), 1132(s), 1101(vs), 1059(vs), 1028(vs), 982(vs), 943(s), 919(s), 893(s), 870(s), 846(m), 800(s), 776(m), 765(vs), 737(s), 648(s), 629(s), 568(s), 567(s), 546(s), 490(s), 477(s), 442(s), 420(s).

2.2.2. $[Cu_4(H_2L)_4] \cdot MeOH$ (**1**·MeOH) and $[Cu_4(H_2L)_4]_2 \cdot 2H_2O \cdot 7MeOH$ (**5**·2H₂O·7MeOH) in mixture.

Solid H₄L (0.3 mmol, 0.068 g) was added to a green solution of $[Cu_2(O_2CMe)_4] \cdot 2H_2O$ (0.15 mmol, 0.060 g) in MeOH (10 mL). The color of the solution immediately changed to dark green. The final solution was stirred under heating at ~ 40 °C for half hour and left for slow evaporation. X-ray quality blue crystals of **1**·MeOH and light blue crystals of **5**·2H₂O·7MeOH were formed after 10 days. The crystals were separated manually under the microscope.

2.2.3. $[Cu_4(H_2L)_4] \cdot MeOH$ (**1**·MeOH)

A yellow solution of H₄L (0.3 mmol, 0.068 g) in MeOH (5 mL) was added to a green solution of $Cu(acac)_2$ (0.30 mmol, 0.079 g) in dmf (20 mL) which was stirred under heating at ~ 90 °C. The resulting dark green solution was refluxed for 3 h and after cooled at r.t. was layered with Et₂O. X-ray quality blue crystals of **1**·MeOH were formed after 3 weeks. The identity of the crystals was confirmed by unit cell determination ($a = b = 17.414(1)$, $c = 16.751(1)$ Å, $\alpha = \beta = \gamma = 90^\circ$, $V = 5079$ Å³). The crystals were filtered off and dried under vacuum. (Yield: 0.056 g, ~ 65 %). The solid was analyzed as solvent free. $C_{44}H_{52}Cu_4N_4O_{16}$ requires: C, 46.07; H, 4.57;

N, 4.88 %. Found: C, 45.88; H, 4.54; N, 4.85 %. FT-IR (KBr pellets, cm^{-1}): 3413(br,s), 2912(w), 2873(w), 2828(w), 1625(vs), 1603(s), 1543(s), 1473(s), 1448(s), 1399(m), 1385(m), 1338(m), 1300(vs), 1254(m), 1206(m), 1160(m), 1129(m), 1083(m), 1029(s), 980(w), 936(w), 915(m), 875(m), 770(s), 683(s), 633(m), 586(m), 489(m), 454(m).

2.2.4. $[\text{Cu}_2(\text{O}_2\text{CMe})_2(\text{H}_3\text{L})_2]$ (**2**)

Solid H_4L (0.3 mmol, 0.068 g) was added to a green solution of $[\text{Cu}_2(\text{O}_2\text{CMe})_4]\cdot 2\text{H}_2\text{O}$ (0.15 mmol, 0.060 g) in MeOH (8 mL). The color of the solution immediately changed to dark green. The final solution was stirred under heating at $\sim 40^\circ\text{C}$ for half hour and left for slow evaporation. A blue precipitate was filtered after one week and the light blue filtrate was left for slow evaporation. X-ray quality light blue crystals of **2** were formed after one month, which were filtered off and dried under vacuum. (Yield: 0.065 g, $\sim 63\%$). $\text{C}_{26}\text{H}_{34}\text{Cu}_2\text{N}_2\text{O}_{12}$ requires: C, 45.02; H, 4.94; N, 4.04 %. Found: C, 44.83; H, 4.91; N, 4.01 %. FT-IR (KBr pellets, cm^{-1}): 3321(br,s), 2912(w), 2869(w), 1621(vs), 1601(s), 1542(s), 1472(s), 1446(s), 1396(m), 1371(m), 1340(s), 1302(vs), 1251(m), 1199(s), 1156(s), 1132(s), 1090(s), 1054(s), 1035(vs), 993(w), 980(w), 940(w), 915(m), 900(w), 878(m), 885(m), 824(m), 786(m), 765(s), 740(m), 684(s), 635(w), 584(s), 548(m), 485(m), 462(m), 415(m).

2.2.5. $[\text{Cu}_4(\text{H}_2\text{L})_4(\text{H}_2\text{O})_2]\cdot 1.5\text{dmf}$ (**3** $\cdot 1.5\text{dmf}$).

A yellow solution of H_4L (0.30 mmol, 0.068 g) in dmf (6 mL) was added to a turquoise solution of $\text{Cu}(\text{acac})_2$ (0.30 mmol, 0.079 g) in dmf (20 mL). The immediately formed green solution was refluxed for 3 h and left for slow evaporation. X-ray quality blue crystals of **3** $\cdot 1.5\text{dmf}$ were formed after 2 months, which were filtered off and dried under vacuum. (Yield: 0.053 g, $\sim 60\%$). The solid was analyzed as solvent free. $\text{C}_{44}\text{H}_{56}\text{Cu}_4\text{N}_4\text{O}_{18}$ requires: C, 44.67; H, 4.77; N, 4.73 %. Found: C, 44.49; H, 4.74; N, 4.70 %. FT-IR (KBr pellets, cm^{-1}): 3553(s), 3477(s), 3414(s), 1638(s), 1617(vs), 1578(s), 1553(s), 1533(s), 1462(w), 1413(m),

1384(m), 1355(s), 1275(s), 1189(s), 1020(s), 937(s), 782(s), 684(m), 653(w), 613(s), 480(m), 455(s).

2.2.6. $[Cu_4(H_2L)_4] \cdot MeOH$ (**1**·MeOH) and $[Cu_4(H_2L)_4(H_2O)] \cdot MeOH$ (**4**·MeOH) in mixture.

Solid H_4L (0.3 mmol, 0.068 g) was added to a green solution of $[Cu_2(O_2CMe)_4] \cdot 2H_2O$ (0.15 mmol, 0.060 g) in MeOH (13 mL). The color of the solution immediately changed to dark green. The final solution was stirred under heating at ~ 40 °C for half hour and left for slow evaporation. After two days the vial was closed and left undisturbed to afford blue crystals of **1**·MeOH and light-blue needle-like crystals of **4**·MeOH. The identity of **1**·MeOH was confirmed by unit cell determination ($a = b = 17.035(3)$, $c = 16.840(5)$ Å, $\alpha = \beta = \gamma = 90$ °, $V = 4886$ Å³). The crystals were separated manually under the microscope.

2.3. Single crystal X-ray crystallography

Crystals of **1**·MeOH ($0.41 \times 0.43 \times 0.57$ mm), **2** ($0.07 \times 0.07 \times 0.54$ mm), **3**·1.5dmf ($0.14 \times 0.41 \times 0.45$ mm) and **4**·MeOH ($0.04 \times 0.04 \times 0.26$ mm) were taken from the mother liquor and immediately cooled to -83 °C (**1**·MeOH), -93 °C (**2**) and -113 °C (**3**·1.5dmf and **4**·MeOH). The few isolated crystals of **5**·2H₂O·7MeOH were destroyed into the cryo-crystallography oil (Paratone-N) and were mounted in capillaries. Most of them showed poor diffraction ability at lower 2θ angles which made them unsuitable for data collection. Repeating efforts to improve the quality of the crystals of **5** proved unsuccessful thus the 'best' quality crystal ($0.08 \times 0.08 \times 0.32$ mm) was used to establish the gross structure of **5**. Collimators of appropriate size were used for each studied crystal i.e. 0.8 for **1** and **2**, 0.5 for **3** and **5** and 0.3 for **4**. Diffraction measurements for all structures were made on a Rigaku R-Axis SPIDER Image Plate diffractometer using graphite monochromated Cu K α radiation. Data collection (ω -scans) and processing (cell refinement, data reduction and Empirical absorption correction) were performed using the CrystalClear program package [32]. The structures were solved by direct methods using SHELXS-97 and refined by full-matrix least-

squares techniques on F^2 with SHELXL ver.2014/6 [33]. Important crystallographic and refinement data for **1**·MeOH, **2**, **3**·1.5dmf and **4**·MeOH are listed in Table 1. Hydrogen atoms were either located by difference maps and were refined isotropically or were introduced at calculated positions as riding on bonded atoms. All non-hydrogen atoms were refined anisotropically. Plots of the structure were drawn using the Diamond 3 program package [34]. Crystallographic data for **5**·2H₂O·7MeOH: C₈₀H₈₄Cu₈N₈O₃₂, fw = 2177.87, triclinic, *P*-1, *a* = 10.8953(2), *b* = 16.6292(3), *c* = 17.4705(3) Å, α = 116.322(1), β = 90.301(1), γ = 93.192(1)°, *V* = 2831.13(9) Å³, *Z* = 1, 14463 reflections collected of which 4699 were used for the refinement of 438 parameters.

Table 1. Crystallographic data for **1**·MeOH, **2**, **3**·1.5dmf and **4**·MeOH.

	1 ·MeOH	2	3 ·1.5dmf	4 ·MeOH
Formula	C ₄₅ H ₅₆ Cu ₄ N ₄ O ₁₇	C ₂₆ H ₃₄ Cu ₂ N ₂ O ₁₂	C _{48.5} H _{66.5} Cu ₄ N _{5.5} O _{19.5}	C ₄₅ H ₅₈ Cu ₄ N ₄ O ₁₈
<i>F</i> _w	1179.09	693.63	1292.73	1197.11
Space group	<i>I</i> ₄ <i>1/a</i>	<i>P</i> 2 ₁	<i>C</i> 2/ <i>c</i>	<i>P</i> -1
<i>a</i> (Å)	17.0529(3)	7.1096(1)	24.5751(4)	10.3714(2)
<i>b</i> (Å)	17.0529(3)	18.8623(3)	16.2214(3)	15.0019(3)
<i>c</i> (Å)	16.8166(3)	10.3396(2)	18.3146(3)	17.5737(3)
α (°)	90	90	90	68.150(1)

β (°)	90	105.711(1)	129.894(1)	74.349(1)
γ (°)	90	90	90	71.783(1)
V (Å ³)	4890.29(19)	1334.77(3)	5601.54(18)	2373.89(8)
Z	4	2	4	2
T (°C)	-83	-93	-113	-113
Radiation	Cu K α (1.54178 Å)	Cu K α (1.54178 Å)	Cu K α (1.54178 Å)	Cu K α (1.54178 Å)
ρ_{calcd} , g cm ⁻³	1.601	1.726	1.533	1.675
μ , mm ⁻¹	2.603	2.591	2.368	2.707
$2\theta_{\text{max}}$ (°)	143.5	130	130	120
parameters refined	214	387	461	657
reflections collected/unique /used	22600/2361 /2361	18009/4330 /4330	30801/4686 /4686	36140/6626/ 6626
R_{int}	0.0370	0.0438	0.0323	0.0628
$(\Delta/\sigma)_{\text{max}}$	0.043	0.001	0.065	0.001
$(\Delta\rho)_{\text{max}}/(\Delta\rho)_{\text{min}}$ (e/Å ³)	0.656/-0.257	0.374/-0.486 e/Å ³	1.255/-0.462 e/Å ³	1.556/-1.303
Reflections with $I > 2\sigma(I)$	2303	4183	4425	4314
R_1^a [$I > 2\sigma(I)$]	0.0330	0.0307	0.0396	0.0765
wR_2^a [$I > 2\sigma(I)$]	0.0897	0.0760	0.1134	0.1871
R_1^a (for all data)	0.0337	0.0319	0.0414	0.1127
wR_2^a (for all data),	0.0902	0.0898	0.0414	0.2431

^a $w = 1/[\sigma^2(F_o^2) + (aP)^2 + bP]$ and $P = (\max(F_o^2, 0) + 2F_c^2)/3$, (a = 0.0451, b = 11.7273 (1); a = 0.0367, b = 0.5167

(2); a = 0.0635, b = 16.7529 (3); a = 0.1347, b = 0.0000 (4)),

$R_1 = \Sigma(|F_o| - |F_c|) / \Sigma(|F_o|)$ and $wR_2 = \{\Sigma[w(F_o^2 - F_c^2)^2] / \Sigma[w(F_o^2)^2]\}^{1/2}$.

3. Results and Discussion

3.1 Synthesis and infrared characterization

The reaction of two equivalents of H₄L with one equivalent of [Cu₂(O₂CMe)₄].2H₂O in MeOH gave a dark green solution which was left for slow evaporation to afford mixture of blue crystals of **1** and light-blue crystals of **5**. The same reaction mixture, albeit more diluted, gave after slow evaporation, mixture of blue crystals of **1** and light-blue crystals of **4**. Complexes **1** and **4** consist of neutral cubane entities, [Cu₄(H₂L)₄] and [Cu₄(H₂L)₄(H₂O)] respectively, whereas complex **5** consists of two cubanes [Cu₄(H₂L)₄] linked through two long Cu-OH bonds involving the pendant alkoxo groups of the Schiff base ligands. A more concentrated reaction mixture, initially gave a blue precipitate which was filtered off and then afforded light-blue crystals of the dinuclear complex **2** after slow evaporation. It is evident that a multitude of products can be isolated from the respective reaction solution depending on their solubility. Complexes **1**, **4** and **5** contain tetranuclear cubane entities, constructed from the Schiff base ligands only, whereas the acetates are involved only in the structure of the dinuclear complex **2**. Therefore, it was attempted to prepare the cubane complexes by using other copper(II) salts following 'rational' synthetic procedures. By using Cu(acac)₂ as the metal source, the cubane complex **1** was isolated in pure form, from the 1:1 [Cu(acac)₂]/H₄L molar ratio reaction in MeOH/dmf. The same reaction in dmf afforded another cubane complex, [Cu₄(H₂L)₄(H₂O)₂], **3**.

The IR spectra of **1**, **2** and **3** which were isolated in pure form were recorded. All spectra exhibit broad bands at ~3400 cm⁻¹ attributed to the ν(OH) vibrations due to the presence of the alkoxo groups of the Schiff base ligands. The ν(C=N) and ν(C-O) stretching vibrations of the Schiff base ligands are observed at ~1620 and ~1350 cm⁻¹. The stretching vibrations of the α-substituted aromatic ring are observed as set of peaks in the 1600-1400 cm⁻¹ region and the out-of-plane CH deformation vibrations at ~760 cm⁻¹. The ν_{as}(C=O) and ν_s(C=O) vibrations of the acetates in **2** are also expected in the 1600-1400 cm⁻¹ region. Both acetates present different coordination modes, one behaves as monoatomic bridge asymmetrically coordinated to the two metal ions and the second behaves as monodentate ligand and also participates in

strong hydrogen bonding (*vide infra*). The peaks at 1597 and 1373 cm^{-1} ($\Delta = 224 \text{ cm}^{-1}$) can be attributed to the $\nu_{\text{as}}(\text{C}=\text{O})$ and $\nu_{\text{s}}(\text{C}=\text{O})$ vibrations of the monodentate acetate, and these at 1538 and 1340 cm^{-1} ($\Delta = 198 \text{ cm}^{-1}$) can be attributed to the $\nu_{\text{as}}(\text{C}=\text{O})$ and $\nu_{\text{s}}(\text{C}=\text{O})$ vibrations of the monoatomic bridge [35].

3.2. Description of the structures

Compound **1** crystallizes in the tetragonal space group $I4_1/a$. The structure consists of neutral tetranuclear entities, $[\text{Cu}_4(\text{H}_2\text{L})_4]$ which possess four-fold rotoinversion symmetry, and one solvate methanol molecule per formula unit, which occupy ca. 9% of the unit cell volume ($\sim 445 \text{ \AA}^3$). The cubane structure of **1** has been previously reported and will be discussed briefly [36,37]. The Cu^{II} ions are coordinated by the tridentate Schiff base ligands, forming a tetranuclear Cu_4O_4 cubane-like configuration. The charge balance is achieved by doubly deprotonation of the Schiff base i.e. of the phenolato hydroxyl group and one of the terminal hydroxyl groups of the ligand. The Cu^{II} ion adopts a CuNO_4 distorted square-pyramidal coordination environment (Figure S1, Table S1). The hydroxyl groups of the Schiff base ligands play three roles in the present structure. O(1) is deprotonated and is coordinated to Cu(II) ions, O(3) configures the intracluster arrangement of the four coordinated Schiff bases through the intramolecular O(3)-H(3O) \cdots O(4) hydrogen bonds whereas the lattice structure of **1** is developed through the intermolecular O(2)-H(2O) \cdots O(3) hydrogen bonds (Figure 1a, Table 2). Each cubane unit is linked through these hydrogen bonds with four neighboring cubanes in a distorted tetrahedral arrangement thus acting as 4-connected node (Figure 1a). The 3D architecture of compound **1** is based on these tetrahedra, which form layers through corner sharing parallel to the (001) plane. These layers are stacked along c axis and two successive layers are rotated by 90° with respect to each other and interpenetrate. The channels formed between the layers are filled by the solvent molecules.

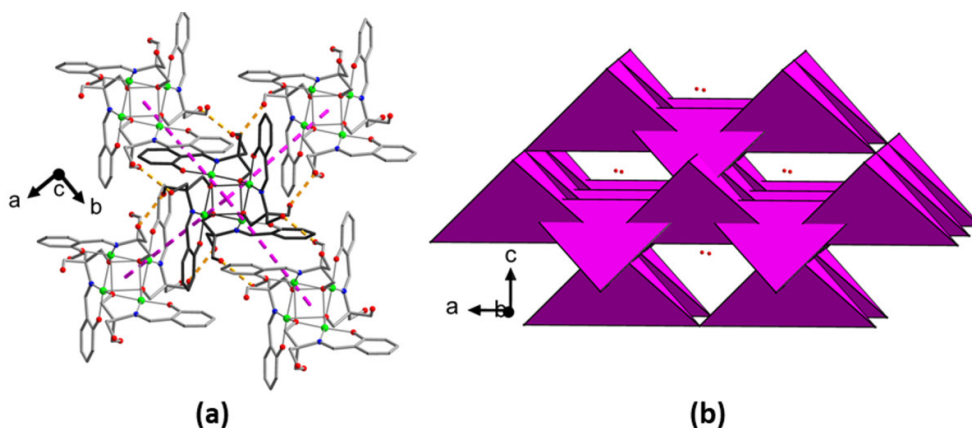


Figure 1. (a) A cubane, shown with dark gray bond color, with its four neighbors connected through hydrogen bonds [O(2)-H(2O)···O(3) dashed orange lines) and forming a distorted tetrahedron, indicated by the pink dashed lines (b) The 3D architecture of tetrahedra of cubane units in the structure of compound **1**. Red dots among the layers indicate the site of lattice solvent methanol molecules.

The molecular structure of **2** consists of neutral dinuclear entities [Cu₂(O₂CMe)₂(H₃L)₂] (Figure 2) with the copper atoms coordinated with one acetate and one Schiff base ligands each presenting different coordination modes. One of the Schiff base ligands, possessing O(4), N(1) and O(1) atoms (Figure 2), chelates to Cu(2) through the phenolato oxygen O(4), the imino nitrogen N(1) and one of the terminal hydroxyl groups O(1). The second ligand chelates to Cu(1) in a similar manner, through O(24), N(21) and O(21) atoms and in addition the phenolato oxygen O(24), serves as bridge to Cu(2) (Figure 2, Scheme 1). One of the acetate ligands (the one defined by O(51) and O(52) atoms) coordinates to Cu(1) with O(51) oxygen in a monodentate fashion whereas the second (the one possessing O(41) and O(42) atoms) serves as monodentate bridge between the two metal ions, through the O(41) atom. The abovementioned coordination of both type of ligands around the Cu^{II} ions promotes the formation of a distorted rhombic Cu₂O₂ core [Cu(1)-O(41)-Cu(2)-O(24)-Cu(1)]. The Cu(1)···Cu(2) distance is 3.4244(9) Å. The coordination environment of each Cu^{II} ion is square pyramidal (the trigonality index τ is 0.115 for Cu(1) and 0.153 for Cu(2)). The apical

position of each square pyramid is occupied by O(41) and O(24) for Cu(1) and Cu(2) respectively, with distances Cu(1)-O(41) = 2.496(3) Å and Cu(2)-O(24) = 2.856(3) Å; the latter is close to the sum of the van der Waals radii and can be characterized as weak bond. The bridging phenolato and carboxylato oxygen atoms are asymmetrically coordinated to the Cu^{II} ions (Cu(1)-O(24) = 1.897(3) Å, Cu(2)-O(24) = 2.856(3) Å; Cu(2)-O(41) = 1.947(3) Å, Cu(1)-O(41) = 2.496(3) Å). The Cu-O and Cu-N bond distances in the basal plane are in the range 1.897(3)-1.997(3) Å for Cu(1) and 1.875(3)-1.968(3) Å for Cu(2) (Table S2). The angles within the basal plane are in the range 82.6(1)-95.3(1) ° for Cu(1) and 82.9(1)-96.3(1) ° for Cu(2), whereas those involving the apical positions are in the range 89.7(1)-97.8(1) ° for Cu(1) and 78.8(1)-99.9(1) ° for Cu(2). As the acetate ligands are both deprotonated, charge balance considerations reveal that the Schiff base ligands in **2** are mono-deprotonated only at the phenolato oxygen atom thus the three protonated hydroxyl groups are available for hydrogen bonding interactions. Two intra-molecular hydrogen bonds, O(1)-H(10)···O(52) and O(22)-H(22O)···O(4), contribute to the stabilization of the dinuclear entities (Figure 2, Table 2) and five intermolecular hydrogen bonding interactions create the 3D supramolecular network (Table 2). The intermolecular hydrogen bonding interactions are divided into two groups; those which promote chain formation by the dinuclear entities along the a-axis [O(2)-H(2O)···O(24), O(21)-H(21O)···O(42) and C(2)-H(2B)···O(51), intrachain ones, Figure 3, Table 2] and those which promote the three-dimensional development of the lattice network [O(3)-H(3O)···O(42), O(23)-H(23O)···O(52), interchain ones, Figure 3, Table 2]. The dinuclear units along the chain axis, the a crystallographic one, interact further through π - π interactions (Figures 11b and 11g). The lattice structure of **2** is dense and robust as there are no voids left for solvate incorporation.

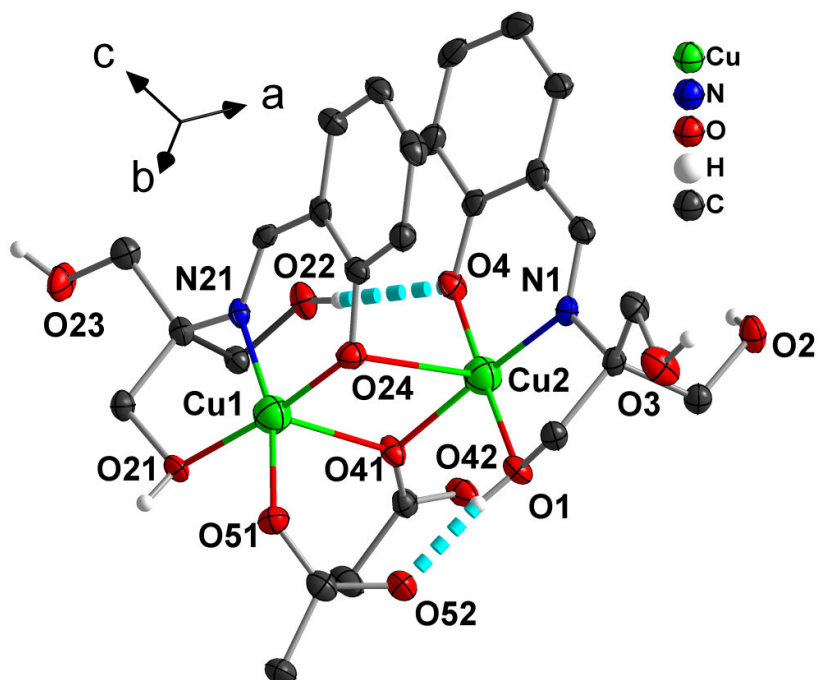


Figure 2. Partially labeled plot of compound 2. Dashed cyan lines indicate intramolecular hydrogen bonds. The thermal ellipsoids are shown at 50% probability. Only hydroxyl hydrogen atoms are shown for clarity.

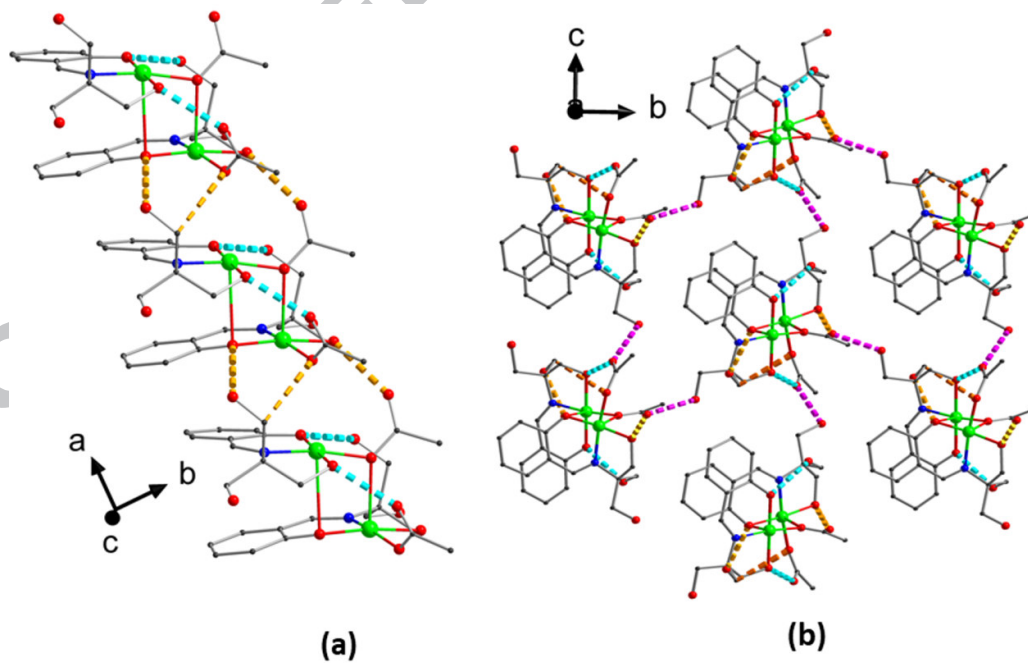


Figure 3. The 3D network in the lattice structure of **2** due to hydrogen bonding interactions. (a) chain formed along a-axis. (b) 3D arrangement of chains. Orange dashed lines indicate interchain O(2)-H(2O)···O(24), O(21)-H(21O)···O(42) and C(2)-H(2B)···O(51) hydrogen bonding interactions and magenta dashed lines indicate O(3)-H(3O)···O(42), O(23)-H(23O)···O(52) interchain ones. Cyan dashed lines indicate intracluster hydrogen bonding interactions.

The molecular structure of **3** is shown in Figure 4. The compound crystallizes in the monoclinic space group $C2/c$. The structure consists of neutral tetranuclear entities, $[\text{Cu}_4(\text{H}_2\text{L})_4(\text{H}_2\text{O})_2]$ which possess two-fold symmetry, and solvate dmf molecules which fill ca. 18% of the unit cell volume ($\sim 1015 \text{ \AA}^3$). The Cu^{II} ions are coordinated by the tridentate Schiff base ligands, forming a tetranuclear Cu_4O_4 cubane-like configuration similar to **1**. The intramolecular $\text{Cu}\cdots\text{Cu}$ distances are in the range 3.1445(8)-3.649(2) \AA (Table S3). Two of the Cu^{II} ions (Cu(1) and Cu(1*)) present CuNO_5 distorted octahedral coordination environment and the other two metal ions (Cu(2) and Cu(2*)) present CuNO_4 square pyramidal coordination with trigonality index τ 0.13. The sixth atom in the coordination sphere of Cu(1) and Cu(1*) ions is an aqua ligand, with the O(1w) forming a rather weak bond equal to 2.820(3) \AA . The Cu-O and Cu-N bond distances in the equatorial plane of the Cu(1) ion, with the distorted octahedron coordination fall in the range 1.905(2)-1.947(2) \AA , whereas those involving the apical positions within the cubane cage are longer due to Jahn-Teller distortion (2.668(2) \AA for Cu(1)-O(2)*, Table S3). The respective bond distances within the basal plane of the Cu(2) ion, with square pyramidal coordination geometry fall in the range 1.913(2)-1.951(2) \AA , whereas a much longer Cu-O bond distance is observed in the apical position (2.526(3) \AA for Cu(2)-O(12)*). The bond angles within the tetragonal plane of the distorted octahedron around Cu(1) and Cu(1') are in the range 83.7(1)-95.4(1) $^\circ$, and those involving the apical positions are in the range 70.1(1)-114.0(1) $^\circ$. The respective angles within

the basal plane of the square pyramidal Cu(2) and Cu(2') are in the range 84.6(1)-95.5(1) °, whereas those involving the apical position are in the range 73.4(1)-122.7(1) °.

The lattice structure of **3** is stabilized by an extensive network of intra- and inter-molecular hydrogen bonding interactions. One intra-molecular hydrogen bonding interaction of the hydroxyl terminal group O(13)-H(13O)···O(1) together with those formed among the water molecules and the oxygen atoms of the terminal hydroxyl groups O(1w)-H(1wA)···O(11) and O(1w)-H(1wB)···O(3) promote the stability of the cubane structure (Figure 4). The cubane units through hydrogen bonding interactions involving the protonated hydroxyl groups O(3)-H(3O)···O(13) promote the formation of chains parallel to the c-axis (Figure 5a). These chains are further linked through hydrogen bonds O(14)-H(14O)···O(1w) involving the hydroxyl groups of the Schiff base as well as the coordinated water molecules, thus creating an overall 3D supramolecular network (Figure 5b, Table 2).

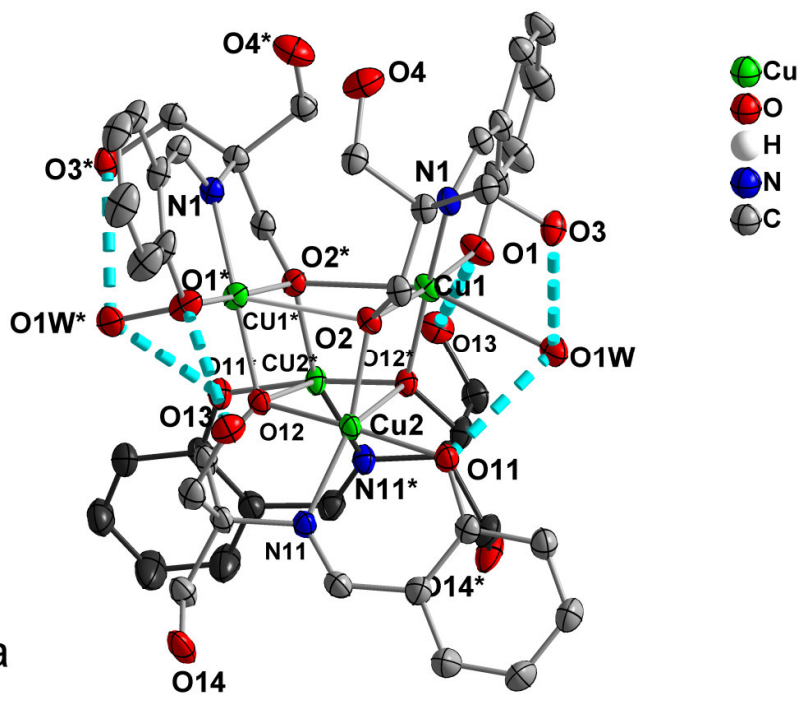


Figure 4. Partially labeled plot of the cubane structure of **3**. Dashed cyan lines indicate O(13)-H(13O)···O(1), O(1w)-H(1wA)···O(11) and O(1w)-H(1wB)···O(3) intramolecular

interactions. The thermal ellipsoids are at 50% probability. Symmetry: (*) $-x, y, 0.5-z$.

Hydrogen atoms have been omitted for clarity.

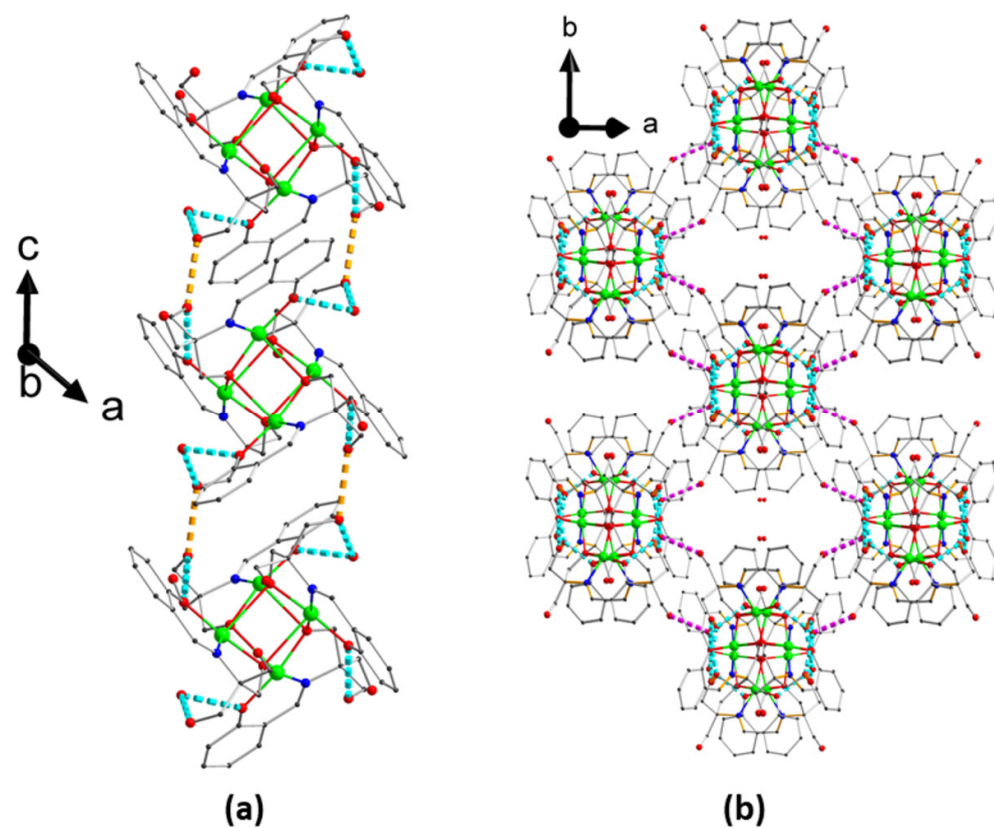


Figure 5. The 3D network in the lattice structure of **3** due to hydrogen bonding interactions. (a) chains of cubane units parallel to the c-axis and (b) linkage of the chains into 3D network. Orange dashed lines indicate O(3)-H(3O)···O13 and magenta lines indicate O(14)-H(14O)···O(1W) interchain ones. Cyan dashed lines indicate intracluster hydrogen bonding interactions.

The molecular structure of **4** is shown in Figure 6. It consists of neutral tetranuclear entities, $[\text{Cu}_4(\text{H}_2\text{L})_4(\text{H}_2\text{O})]$, and MeOH solvate molecules which fill 3.5% of the unit cell volume ($\sim 83 \text{ \AA}^3$). The Cu^{II} ions are coordinated by the tridentate Schiff base ligands, forming a tetranuclear

Cu₄O₄ cubane-like configuration similar to **1** and **3**. The intramolecular Cu...Cu distances are in the range 3.165(2)-3.507(1) Å (Table S4). Two of the Cu^{II} ions (Cu(1) and Cu(2)) present CuNO₅ distorted octahedral coordination environment and the other two metal ions (Cu(3) and Cu(4)) present CuNO₄ square pyramidal coordination with trigonality index τ 0.13 and 0.11, respectively. The sixth coordination site at Cu(1) is completed by a protonated -CH₂OH group of the Schiff base ligand (O(3), Figure 6), whereas in the case of Cu(2) is an aqua ligand (O1w, Figure 6). The Cu-O and Cu-N bond distances in the equatorial plane of the distorted octahedron fall in the range 1.899(5)-1.957(5) Å, whereas those involving the apical positions are much longer due to Jahn-Teller distortion (2.589(4) and 2.712(4) Å for Cu(1) and 2.735(6) and 2.757(5) Å for Cu(2), Table S4). The respective bond distances within the basal plane of the square pyramidal coordination geometry fall in the range 1.901(5)-1.946(5) Å, whereas a much longer Cu-O bond distance is observed in the apical position (2.622(4) Å for Cu(3) and 2.557(5) Å for Cu(4), Table S4). The bond angles within the tetragonal plane of the distorted octahedron around Cu(1) and Cu(2) are in the range 82.3(2)-96.7(2) °, and those involving the apical positions are in the range 67.7(2)-116.5(2) °. The respective angles within the basal plane of the square pyramidal Cu(3) and Cu(4) are in the range 83.4(2)-95.9(2) °, whereas those involving the apical position are in the range 69.8(2)-122.2(2) °.

An extensive network of intra and inter cluster hydrogen bonds is also observed in the lattice structure of compound **4** (Figure 7). The configuration of ligands within the cubane units is due to an extensive intracubane hydrogen bonds interactions involving the protonated and deprotonated hydroxyl terminal groups of the ligands O(3)-H(3O)...O(31), O(13)-H(13O)...O(33), O(24)-H(24O)...O(11) and those involving the hydrogen atoms of coordinated water molecule as well, O(1w)-H(1wA)...O(1) and O(1w)-H(1wA)...O(14). Each cubane cluster interacts from one side with a neighboring one through the O(23)-H(23O)...O(4) hydrogen bonds and from the other side with another one through the hydrogen bonds involving the lattice methanol solvent molecules, O(1M)-H(1OM) ...O(13) and O(33)-H(33O)...O(1M) (Figure 7, Table 2), thus forming chains parallel to the [0,1,1]

direction. The chains interact through O(4)-H(4O)···O(1w), O(34)-H(34O)···O(24) and O(14)-H(14O)···O(3) and build the 3D architecture of compound **4** (Figure 7).

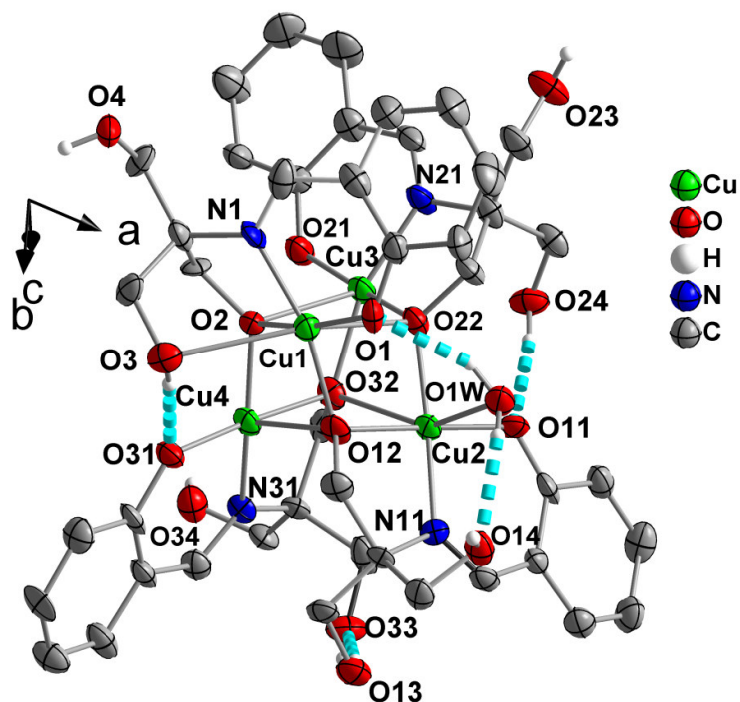


Figure 6. Partially labeled plot of the cubane structure of **4**. Only hydroxyl and water hydrogen atoms are shown for clarity. Dashed cyan lines indicate O(3)-H(3O)···O(31), O(13)-H(13O)···O(33), O(24)-H(24O)···O(11), O(1w)-H(1wA)···O(1) and O(1w)-H(1wA)···O(14) intramolecular interactions. The thermal ellipsoids are at 50% probability.

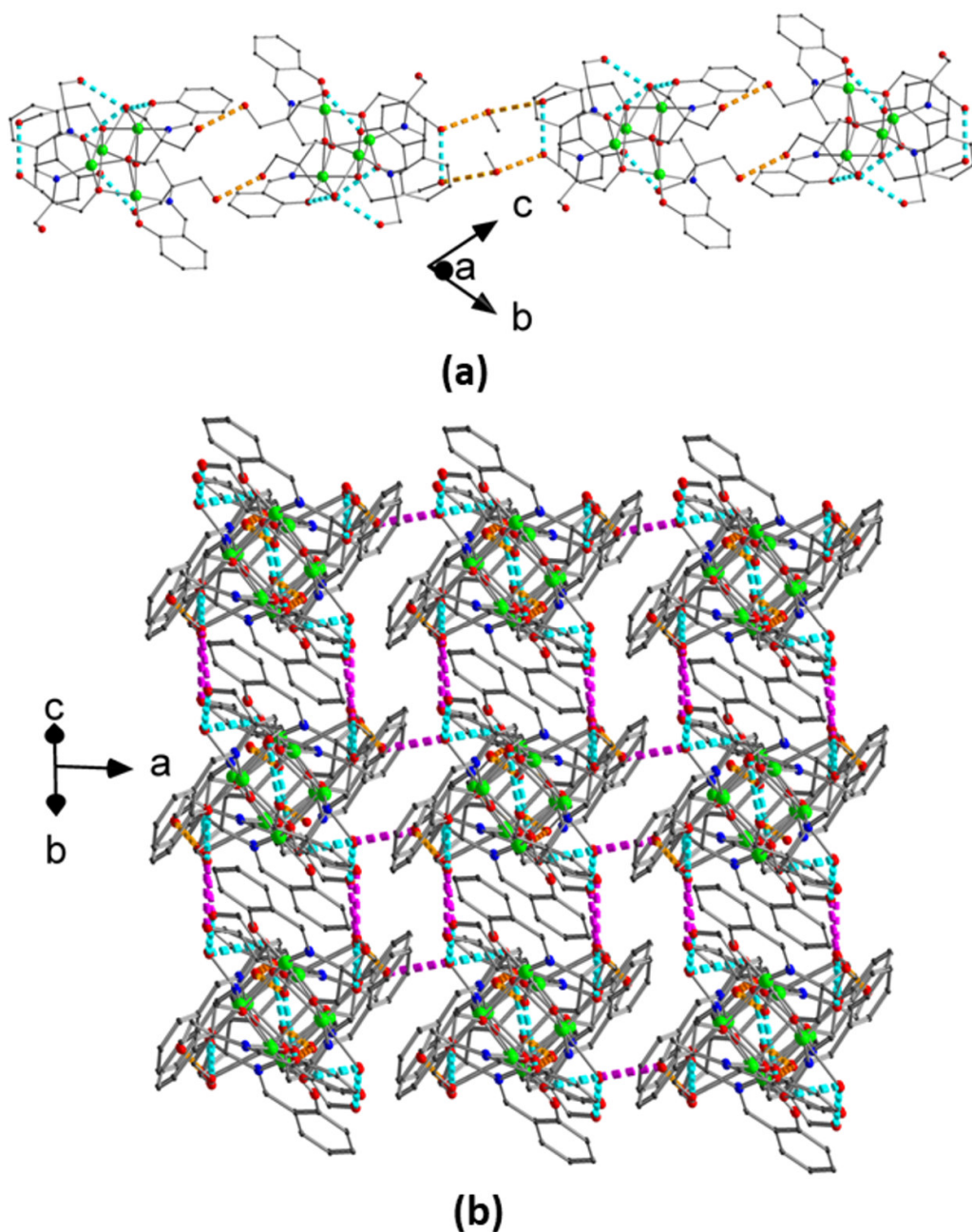


Figure 7. The 3D network in the lattice structure of **4** due to hydrogen bonding interactions. (a) chains of cubane units parallel to the [011] crystallographic direction and (b) linkage of the chains into 3D network. Orange dashed lines indicate O(23)-H(23O)···O(4), O(1M)-H(1OM)···O(13), O(33)-H(33O)···O(1M) and magenta lines indicate O(4)-H(4O)···O(1W), O(34)-H(34O)···O(24) and O(14)-H(14O)···O(3) interchain ones. Cyan dashed lines indicate intracluster hydrogen bonding interactions.

The Schiff base ligands in the cubane structures **1** and **3** are in the doubly deprotonated form at the phenolato oxygen and one of the hydroxyl groups. These ligands behave as tridentate $\mu_3\text{-}\kappa^3\text{O}:\kappa\text{O}':\kappa\text{N}$ and bind to the metal ions through the phenolato oxygen, the imino nitrogen and the deprotonated hydroxo oxygen atoms. The latter is also coordinated to two neighboring Cu^{II} ions, acting as triple bridge between the metal ions, and occupies the oxygen sites of the Cu_4O_4 cubane structure (Scheme 1). Also in **4**, three of the ligands behave as tridentate $\mu_3\text{-}\kappa^3\text{O}:\kappa\text{O}':\kappa\text{N}$ as in **1** and **3**, and the fourth behaves as tetradentate $\mu_3\text{-}\kappa^3\text{O}:\kappa\text{O}':\kappa\text{O}'':\kappa\text{N}$ coordinated to a Cu^{II} ion through the phenolato oxygen, the imino nitrogen, of the protonated hydroxo oxygen and the deprotonated hydroxo oxygen atom which also bridges two neighboring Cu^{II} ions. Finally the Schiff base ligands in **2** are mono deprotonated at the phenolato oxygen atom and present two different coordination modes, chelating through the phenolato oxygen, the imino nitrogen and the protonated hydroxyl group, and bidentate $\mu_2\text{-}\kappa^2\text{O}:\kappa\text{O}':\kappa\text{N}$, coordinated to the adjacent Cu^{II} ion through the bridging phenolato oxygen atom. The molecular structure of **5** is shown in Figure S2. The structure consists of two cubane-like Cu_4O_4 entities, similar to those in **1**, which are linked through long Cu-OH bond distances. The compound crystallizes in the triclinic space group $P\bar{1}$ and is centrosymmetric. The data have been collected from a poorly diffracting crystal and they are useful in deriving the connectivity of compound **5** only. The unit cell contains one cubane dimer, two water and seven methanol solvate molecules. The Schiff base ligands in **5** are also doubly deprotonated as in **1** and **4** and present two different coordination modes. Three of the ligands behave as tridentate $\mu_3\text{-}\kappa^3\text{O}:\kappa\text{O}':\kappa\text{N}$ as in **1** and **4**, and the fourth behaves as tetradentate $\mu_4\text{-}\kappa^3\text{O}:\kappa\text{O}':\kappa\text{O}'':\kappa\text{N}$, coordinated to a Cu^{II} ion from a neighboring cubane unit through a protonated hydroxyl group, thus creating the cubane dimers.

O(21)-H(21O)···O(42)	2.709	1.872	174.0	-1+x, y, z
O(2)-H(2O)···O(24)	2.822	2.024	158.5	1+x, y, z
C(2)-H(2B)···O(51)	3.246	2.473	134.6	1+x, y, z
O(3)-H(3O)···O(42)	2.780	1.957	166.3	2-x, -0.5+y, -z
O(23)-H(23O)···O(52)	2.786	1.989	158.1	x, y, 1+z
3·1.5dmf				
Intramolecular				
O(13)-H(13O)···O(1)	2.637	1.931	178.3	-x, y, 0.5-z
O(1w)-H(1wA)···O(11)	2.804	1.987	170.4	x, y, z
O(1w)-H(1wB)···O(3)	2.894	2.086	177.0	x, y, z
Intermolecular				
O(3)-H(3O)···O(13)	2.690	1.953	167.9	-x, 1-y, 1-z
O(14)-H(14O)···O(1w)	2.739	2.142	171.9	-0.5+x, 0.5-y, -0.5+z
4·MeOH				
Intramolecular				
O(3)-H(3O)···O(31)	2.696	1.86	170.6	x, y, z
O(13)-H(13O)···O(33)	2.704	1.87	171.4	x, y, z
O(24)-H(24O)···O(11)	2.668	1.84	170.7	x, y, z
O(1w)-H(1wA)···O(1)	2.797	1.98	154	x, y, z
O(1w)-H(1wB)···O(14)	2.758	2.06	162	x, y, z
Intermolecular				
O(23)-H(23O)···O(4)	2.729	1.90	169.4	-x+1, -y+1, -z
O(1m)-H(1Om)···O(13)	3.019	2.54	117.4	x, y-1, z
O(33)-H(33O)···O(1m)	2.709	1.9	147.1	-x+1, -y+1, -z+1
O(4)-H(4O)···O(1w)	2.668	1.85	165.5	x-1, y, z
O(34)-H(34O)···O(24)	2.704	1.92	161	-x+1, -y+1, -z+1
O(14)-H(14O)···O(3)	2.691	1.88	161.0	-x+1, -y+2, -z

3.3 Hirshfeld surface analysis

The crystal packing and the intermolecular interactions of structures **1**, **2**, **3** and **4** are further studied by the Hirshfeld Surface (HS) analysis method tools [38]. In Figure 8a the HS for compound **1** decorated with d_{norm} property is presented. Figure 8b and 8c present the

fingerprint plots with the contribution for all the interactions and only for O...H interactions respectively, for the same compound. In Figure 8c and in analogous Figures in the rest of the text (Figures-9d, 9e, 10c, 10d, 11f and 11g) the contributions from all the interactions in the respective fingerprint plots are within the gray area beneath the respective type of interactions, which are indicated with the colored area. The green lines [39] correspond to the $d_i + d_e$ distances which are equal to the sums of the van der Waals (vdW) radii [40] of the corresponding pairs of atoms involved in the specific interaction and so all the points for each type of interaction which are located within the cyan area indicate strong interactions i.e. $d_i + d_e$ sums with values smaller than sum of the corresponding vdW radii. The analysis of fingerprint plots give 47.2, 29.9 and 17.4 % contributions from H...H, O...H/H...O and C...H/H...C interactions respectively for compound **1**. The strongest contribution comes from the O...H/H...O type of interactions and the red spots B1 and B1' in Figure 8a indicate the acceptor O(3) and the H(20) atom of the donor O(2) atoms respectively, in the O(2)-H(20)...O(3) hydrogen bonds. Through these interactions other parts of molecules are coming closer, as the one indicated with faint red spots on the d_{norm} HS and are enclosed by the black and gray circles in Figure 8a, which correspond to the acceptor O(2) (B2 points) and to H(8) hydrogens (B2' points) of the C(8) donor atoms in the C(8)-H(8)...O(2)ⁱ hydrogen bonds [(i):0.5-x, 0.5-y, 1.5-z; C(8)-H(8)...O(2)ⁱ: 0.85, H(8)...O(2)ⁱ: 2.64, C(8)...O(2)ⁱ:3.412, C(8)-H(8)-O(2):152°] respectively. Both of these interactions contribute at the spikes B and B' in Figures 8b and 8c. In Figure 8b, A indicate the contribution of H...H conduct points and C/C' the C...H/H...C ones respectively. Based on fingerprint plot analysis for compound **3**, the contribution for H...H, C...H/H...C, O...H/H...O type of interactions are 47.9, 25.3 and 18.6 % respectively (Figure 9c). In the d_{norm} presentation (Figure 9a) of HS for compound **3** the intense red spots B1 and B2 correspond to the acceptor atoms O(13) and O(1W) and the primed ones B1' and B2' correspond to the hydrogen atoms of donors O(3) and O(14), of the following hydrogen bonds O(3)-H(3O)...O(13) and O(14)-H(14O)...O(1w). These hydrogen bond interactions contribute to the spikes observed in the fingerprint plots at points B and B'

(Figure 9c and d) and are quite strong as the most of the points lie in the area below the green line (Figure 9d). These interactions bring closer other parts of the clusters such as B3 [acceptor atom O(14)] and B3' [hydrogen H(3) of the donor atom C(3)] through the weak hydrogen bond C(3)-H(3)···O(14). Also H(11A) and H(22) hydrogen atoms of C(11) and C(22) carbon atoms interact with the phenyl ring C(21)···C(26) and C(1)···C(6) respectively resulting in C-H··· π interactions, indicated with the circled areas in the HS decorated with Shape index (Figure 9b), where the complementary hollows (red) and bumps (blue) areas are parts of the HSs where neighboring molecules touching each other through C-H··· π interactions [41]. The asymmetry distribution of points in the area of donors conduct points and more specifically at points B'' (Figures 9c and 9d), in comparison to those of the acceptors is indicative that at these points contribute different molecules i.e. those of lattice solvents (B'' red point in Figure 9a). For compound **4**, the contribution for H···H, C···H/H···C, O···H/H···O type of interactions are 57.6, 19.9 and 19.9 % respectively (Figure 10b). In the d_{norm} representation (Figure 10a) the hydrogen bonds O(4)-H(4)···O(1W), O(14)-H(14)···O(3) and O(23)-H(23)···O(4) give the red intense spots B1, B2, and B3 for the acceptor oxygen atoms O(1W), O(3) and O(4) and the B1', B2', and B3' ones for the corresponding hydrogen atoms of the donors O(4), O(14) and O(23) respectively. These hydrogen bond interactions contribute to the spikes observed in the fingerprint plots at points B and B' (Figure 10b and c) and are quite strong as the most of the points lie in the cyan area below the green line (Figure 10c). The points B5 and B4' in Figure 10a indicate the O13 (acceptor) and H33O (hydrogen of donor O33 atom) for the hydrogen bonds O1M-H10M···O13 and O33-H33O···O1M respectively. For this structure the C-H··· π type of interactions contribute effectively as indicated with the presence of points at the cyan area below the green line in Figure 10d.

The basic building block for the 3D structures of compounds **1**, **3** and **4** are the structural units with a cubane core and depending on the presence of water molecules (two in the case of compound **3** and one in the case of compound **4**) or not (compound **1**) present different

packing arrangements, but all of them have a common characteristic. More specifically the atoms O(3) (Figure S1, point B1 in Figure 8a) for compound **1**, O(13) and O(1W) (Figure 4, points B1 and B2 in Figure 9a) for compound **3** and O(3) and O(1W) (Figure 6, points B1 and B2 in Figure 10a) for compound **4**, all of them are distributed around the middle of each cluster and act as donors in the respective intracluster interactions (Table 2) and in parallel as acceptors for the intercluster ones (Table 2). In all three clusters the donor atoms are the oxygen atoms from non coordinated hydroxyl terminal groups of the Schiff base. In the case of compound **1** these groups participate only in intercluster interactions but in the case of compounds **3** and **4**, they interact with the lattice solvent molecules (points B'' and B4', B5 in Figures 9a and 10a respectively). Concluding the Schiff base used for this study could be used as structural units to engineer lattices which could act simple as hosts (compound **1**) or as functionalized host lattices (compound **3** and **4**).

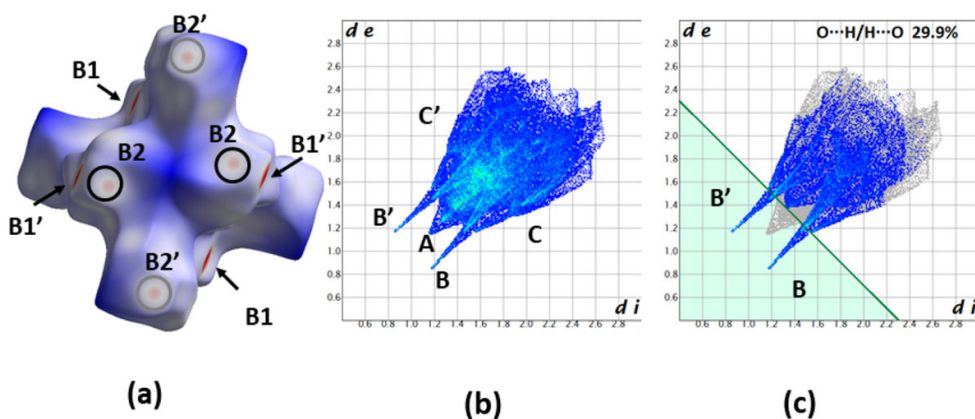


Figure 8. Hirshfeld surface analysis plots for compound **1**. (a) HS decorated with d_{norm} property. B1 and B2 points indicate the acceptor O(3) and O(2) atoms in the O(2)-H(2O)···O(3) and C(8)-H(8)···O(2) hydrogen bonds respectively. B1' and B2' indicate the hydrogen atoms H(2O) and H(8) in the respective hydrogen bonds. Fingerprint plots : (b) for all type of interactions and (c) decomposed ones only for O···H/H···O type of interactions . A (in (b)) indicate H···H conduct points. B and B' (in (b) and (c)) indicate the areas of contribution of conducts to the acceptor atoms and respective conducts to the Hydrogen atoms

bonded to the donor ones in the $O\cdots H/H\cdots O$ type of interactions. C and C' indicate the analogous areas for $C\cdots H/H\cdots C$ interactions.

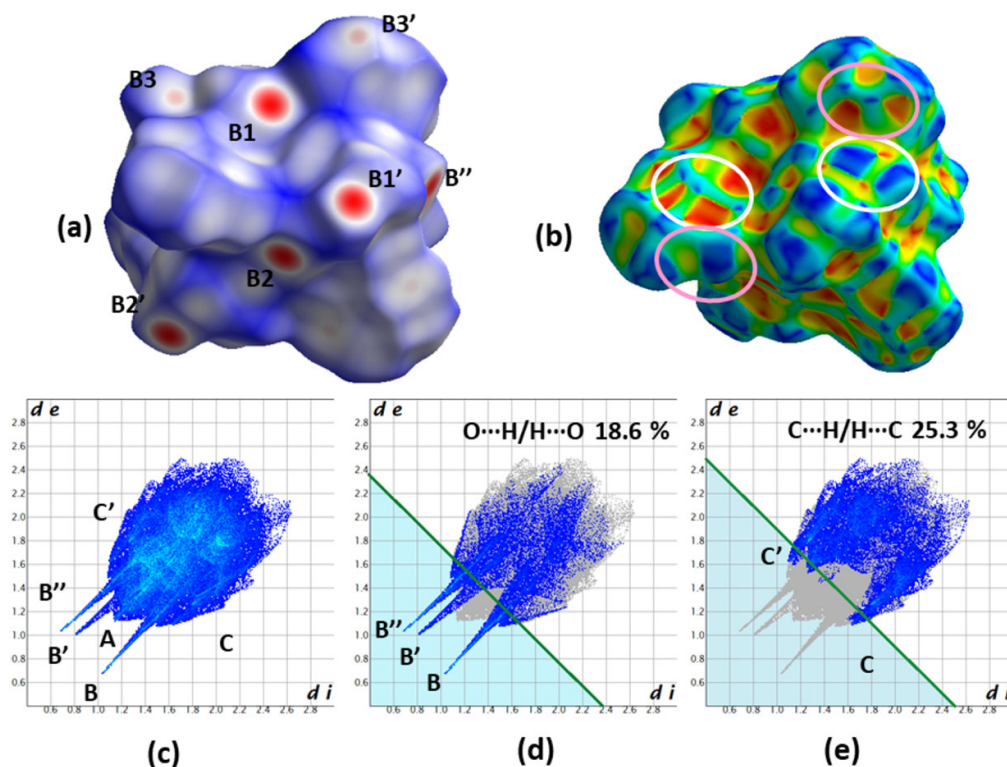


Figure 9. Hirshfeld surface analysis plots for compound **3**. (a) HS decorated with d_{norm} property. B1, B2 and B3 indicate the acceptor O(13), O(1W) and O(14) atoms in the $O(3)-H(3O)\cdots O(13)$, $O(14)-H(14O)\cdots O(1W)$ and $C(3)-H(3)\cdots O(14)$ hydrogen bonds respectively and B1', B2' and B3' indicate the hydrogen atoms H(3O), H(14O) and H(3) in the same hydrogen bonds. (b) HS decorated with Shape index. The white and pink ellipses indicate the weak $C\cdots H/H\cdots C$ interactions of $C-H\cdots\pi$ type i.e. C(11)-H(11A) and C(22)-H(22) with the phenyl ring C(21)...C(26) and C(1)...C(6) respectively. Fingerprint plots: (c) for all type of interactions, and decomposed ones (d) for $O\cdots H/H\cdots O$ and (e) for $C\cdots H/H\cdots C$ type of interactions. A in (c) indicate areas of $H\cdots H$ contact points. B, B' [in (c), (d)] and C, C' [in (c), (e)] indicate areas with contacts to the acceptor atoms (unprimed ones) and areas (the

primed ones) with conducts to Hydrogen atoms of $O\cdots H/H\cdots O$ and $C\cdots H/H\cdots C$ type of interactions respectively.

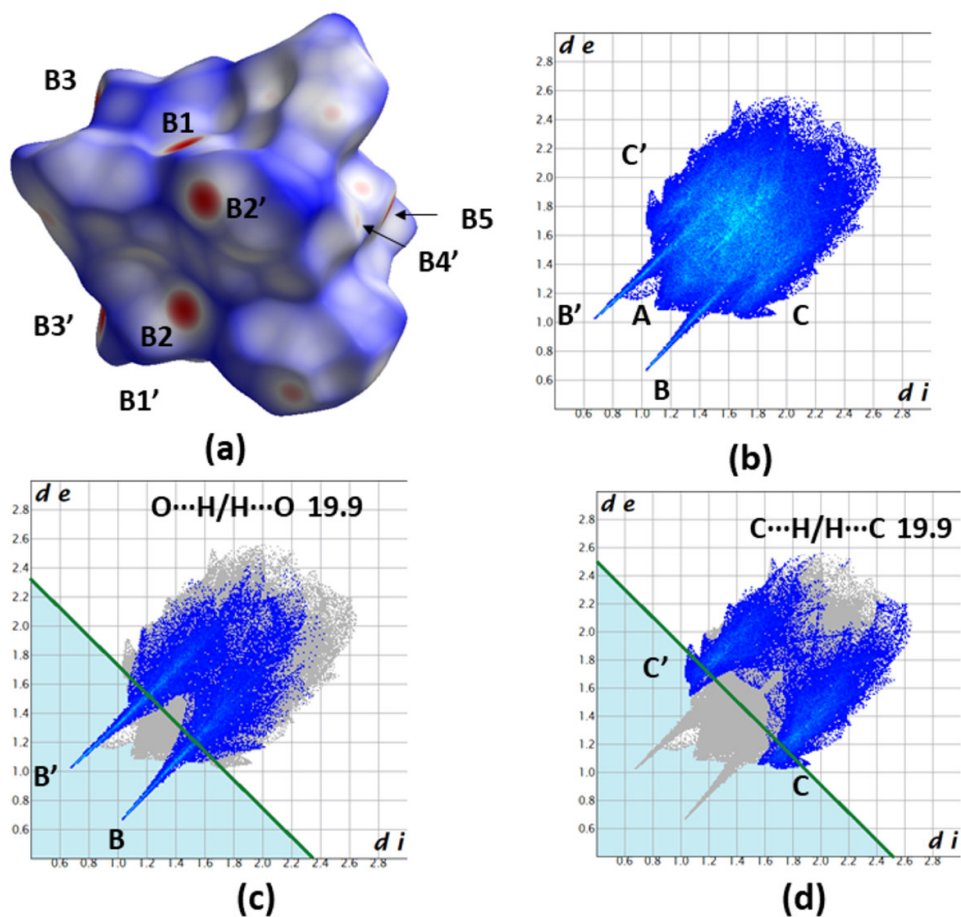


Figure 10. Hirshfeld surface analysis plots for compound **4**. (a) HS decorated with d_{norm} property. B1, B2 and B3 indicate the acceptor O(1W), O(3) and O(4) in the $O(4)\cdots H(4)\cdots O(1W)$, $O(14)\cdots H(14)\cdots O(3)$ and $O(23)\cdots H(23)\cdots O(4)$ hydrogen bonds respectively. B1', B2' and B3' indicate the hydrogen atoms H(4O), H(14O) and H(23O) in the respective hydrogen bonds. B5 and B4' indicate the O13 (acceptor) and H33O (hydrogen of donor O33 atom) for the following hydrogen bonds $O1M\cdots H10M\cdots O13$ and $O33\cdots H33O\cdots O1M$. Fingerprint plots: (b) for all type of interactions and decomposed ones (c) for $O\cdots H/H\cdots O$ and (d) for $C\cdots H/H\cdots C$ type of interactions. A in (c) indicate areas of $H\cdots H$ conduct points.

B, B' [in (b), (c)] and C, C' [in (c), (d)] indicate areas with conducts to the acceptor atoms (unprimed ones) and areas (the primed ones) with conducts to Hydrogen atoms of $O\cdots H/H\cdots O$ and $C\cdots H/H\cdots C$ type of interactions respectively.

The basic structural units in compound **2** are the dinuclear complexes shown in Figure 3 and present differences in their intermolecular interactions with respect to the other three compounds studied in the present work. Based on fingerprint plot analysis of HS for compound **2** the contribution for $H\cdots H$, $O\cdots H/H\cdots O$, $C\cdots H/H\cdots C$ and $C\cdots C$ type of interactions are 58.6, 28.9, 6.2 % and 2.8 % respectively (Figure 11e). Figure 11a and 11b present two views of the HS for compound **2** decorated with d_{norm} values and the intense red points B1, B2, B3, B4 and B5 correspond to the acceptor oxygen atoms and the primed one B1', B2', B3', B4' and B5' to the hydrogen atoms of the donors for the hydrogen bonds $O(21)-H(21O)\cdots O(42)$, $O(2)-H(20)\cdots O(24)$, $C(2)-H(2B)\cdots O(51)$, $O(3)-H(30)\cdots O(42)$ and $O(23)-H(230)\cdots O(52)$. These hydrogen bond interactions contribute to the spikes observed in the fingerprint plots at points B and B' (Figure 11e and f) and are quite strong as the most of the points lie in the cyan area below the green line (Figure 11f). In this case only the O(24) (B2 point) act as an acceptor atoms from the hydroxyl groups of the Schiff base and all other acceptor oxygen atoms belong to the deprotonated acetate oxygen atoms (O42, O51 and O52, Figure 2). The views of HS presented in Figures 11a and 11b are along $-a$ and along a axis respectively, so these views present the dinuclear units down and opposite to direction of the stacking axis (Figure 3a). Figures 11c and 11d present the HS of compound **2** decorated with Shape index, and are the same views as those presented in Figures 11a and 11b. The circles in Figures 11c and 11d indicate areas on the HSs with the characteristic blue and red triangles for $\pi\cdots\pi$ interactions (Figure 11g).

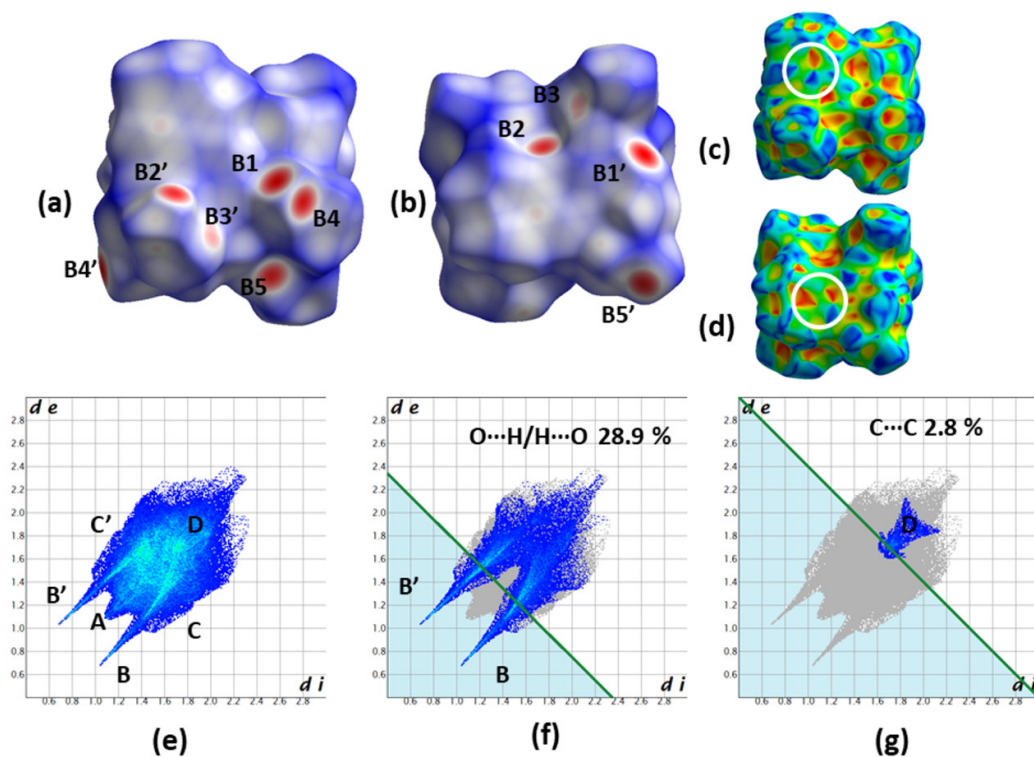


Figure 11. Hirshfeld Surface analysis plots for compound **2**. (a) HS decorated with d_{norm} property and shown along the direction of $-a$ and (b) along the a axis. B1, B2, B3, B4 and B5 indicate the acceptor oxygen atoms O(42), O(24), O(51), O(42) and O(52) in the hydrogen bonds O(21)-H(210) \cdots O(42), O(2)-H(20) \cdots O(24), C(2)-H(2B) \cdots O(51), O(3)-H(30) \cdots O(42) and O(23)-H(23O) \cdots O(52) respectively. B1', B2', B3', B4' and B5' indicate the hydrogen atoms in the same hydrogen bonds. (c) HS decorated with the Shape index property and shown along the direction $-a$ and in (d) along the a axis. The circled areas indicate contact points through $\pi \cdots \pi$ interactions. Fingerprint plots: (e) for all type of interactions and decomposed ones for O \cdots H/H \cdots O type (f) and C \cdots C type ones (g). A in (e) indicate H \cdots H contact points. B, B' [in (e) and (f)] indicate areas with contacts to the acceptor atoms and areas with contacts to Hydrogen atoms of O \cdots H/H \cdots O type of interactions respectively. D in (e) and (g) indicate the contribution from C \cdots C type of interactions.

c) and d) the same views of HS as in a) and b) respectively decorated with Shape index. Fingerprint plots for all the interactions (e)) and in the decomposed presentation for O...H/H...O (f)) and C...C (g)) type of interactions for compound 2. A and D indicate H...H and C...C conduct points. B, C and the primed ones B', C' indicate the corresponding acceptor and Hydrogen's atoms of donors in O...H/H...O and C...H/H...C interactions. See text for details.

4. Conclusions

Five Cu(II) cluster compounds using the Schiff base ligand OH-C₆H₄-CH=NC(CH₂OH)₃ have been synthesized and have been studied with single crystal methods and spectroscopic techniques. Interestingly the Schiff base ligands present a variety of coordination modes with Cu(II) cations, such as tridentate and tetradentate depending on the degree of deprotonation (mono or doubly) and on the presence or not of other ligands connected with metal core unit of each studied cluster. This flexibility of the Schiff base ligand results in five coordination modes. Also the combined detailed crystallographic study of intermolecular interactions together with the Hirshfeld Surface analysis reveal that the building blocks (cubane units in 1, 3, 4 and 5 and dinuclear unit in 2) use specific common oxygen atoms as acceptors of the hydrogen atoms of the non-coordinated hydroxyl groups and build the different 3D structures observed in the studied compounds. This characteristic make probable their use as building blocks to design structure architectures with potential applications as host lattices.

Appendix A. Supplementary material

The molecular structure of the cubane structure of 1 and 5 (Figures S1, S2) and selected bond distances and angles for 1-4 (Tables S1-S4). CCDC 1838286, 1838287, 1838288 and 1838289 contain the supplementary crystallographic data for 1·MeOH, 2, 3·1.5dmf and

4-MeOH. These data can be obtained free of charge via: <http://www.ccdc.cam.ac.uk/conts/retrieving.html>, or from the Cambridge Crystallographic Data Centre, 12 Union Road, Cambridge CB2 1EZ, UK; fax: (+44) 1223-336-033; or e-mail: deposit@ccdc.cam.ac.uk. Supplementary data associated with this article can be found, in the online version, at doi:

References

- [1] C. A. Trickett, A. Helal, B. A. Al-Maythalyony, Z. H. Yamani, K. E. Cordova, O. M. Yaghi, *Nature Rev. Mater.* 2 (2017) 17045.
- [2] A. Schoedel, M. Li, M. O'Keeffe, O. M. Yaghi, *Chem. Rev.* 116 (2016) 12466.
- [3] C. Pettinari, F. Marchetti, N. Mosca, G. Tosi, A. Drozdov, *Polym. Int.* 66 (2017) 731.
- [4] K. T. Mahmudov, M. N. Kopylovich, M. F. C. Guedes da Silva, A. J. L. Pombeiro, *Coord. Chem. Rev.* 345 (2017) 54.
- [5] R. Bertani, P. Sgarbossa, A. Venzo, F. Lelj, M. Amati, G. Resnati, T. Pilati, P. Metrangolo, G. Terraneo, *Coord. Chem. Rev.* 254 (2010) 677.
- [6] B. Li, S.-Q. Zang, L.Y. Wang, T. C. W. Mak, *Coord. Chem. Rev.* 308 (2016) 1.
- [7] J. Teyssandier, S. De Feyter, K. S. Mali, *Chem. Commun.* 52 (2016) 11465.
- [8] L. Voorhaar, R. Hoogenboom, *Chem. Soc. Rev.* 45 (2016) 4013.
- [9] Y.-F. Han, Y.-X. Yuan, H.-B. Wang, *Molecules* 22 (2017) 266.
- [10] S. G. Telfer, R. Kuroda, *Coord. Chem. Rev.* 242 (2003) 33.
- [11] P. G. Cozzi, *Chem. Soc. Rev.* 33 (2004) 410.
- [12] J.-P. Costes, F. Dahan, W. Wernsdorfer, *Inorg. Chem.* 45 (2006) 5.
- [13] J.-P. Costes, F. Nicodème, *Chem. Eur. J.* 8 (2002) 3442.
- [14] J.-P. Costes, F. Dahan, F. Nicodème, *Inorg. Chem.* 42 (2003) 6556.
- [15] C. Boskovic, R. Bircher, P. L. W. Tregenna-Piggott, H. U. Güdel, C. Paulsen, W. Wernsdorfer, A. L. Barra, E. Khatsko, A. Neels, H. Stoeckli-Evans, *J. Am. Chem. Soc.* 125 (2003) 14046.

- [16] H. Miyakasa, R. Clérac, W. Wernsdorfer, L. Lecren, C. K. S. Bonhomme, M. Yamashita, *Angew. Chem. Int. Ed.* 43 (2004) 2801.
- [17] H. Oshio, N. Hoshino, T. Ito, M. Nakano, *J. Am. Chem. Soc.* 126 (2004) 8805.
- [18] A. M. abu-Dief, I. M. A. Mohamed, Beni-Suef Univ. *J. Basic Appl. Sci.* 4 (2015) 119.
- [19] W. A. Wani, U. Baig, S. Shreaz, R. A. Shiekh, P. F. Iqbal, E. Jameef, A. Ahmad, S. H. Mohd-Setapar, M. Mushtaque, L. T. Hun, *New J. Chem.* 40 (2016) 1063.
- [20] D. P. Kessissoglou, C. P. Raptopoulou, E. G. Bakalbassis, A. Terzis, J. Mrozinski, *Inorg. Chem.* 31 (1992) 4339.
- [21] D. P. Kessissoglou, M. L. Kirk, M. S. Lah, X. Li, C. P. Raptopoulou, W. E. Hatfield, V. L. Pecoraro, *Inorg. Chem.* 31 (1992) 5424.
- [22] M. Dey, C. P. Rao, P. Saarenketo, K. Rissanen, E. Kolehmainen, *Eur. J. Inorg. Chem.* (2002) 2207.
- [23] R. Bircher, B. F. Abrahams, H. U. Güdel, C. Boskovic, *Polyhedron* 26 (2007) 3023.
- [24] J.-W. Ran, S.-Y. Zhang, B. Xu, Y. Xia, D. Guo, J.-Y. Zhang, Y. Li, *Inorg. Chem. Commun.* 11 (2008) 73.
- [25] M. Dey, C. P. Rao, P. K. Saarenketo, K. Rissanen, E. Kolehmainen, P. Guionneau, *Polyhedron* 22 (2003) 3515.
- [26] M. Dey, C. P. Rao, P. K. Saarenketo, K. Rissanen, *Inorg. Chem. Commun.* 5 (2002) 924.
- [27] P. V. Rao, C. P. Rao, A. Sreedhara, E. K. Wegelius, K. Rissanen, E. Kolehmainen, *Dalton Trans.* (2000) 1213.
- [28] C. P. Rao, A. Sreedhara, P. V. Rao, M. B. Verghese, K. Rissanen, E. Kolehmainen, N. K. Lokanath, M. A. Sridhar, J. S. Prasad, *Dalton Trans.* (1998) 2383.
- [29] C. P. Raptopoulou, Y. Sanakis, V. Psycharis, M. Pissas, *Polyhedron* 64 (2013) 181.
- [30] E. C. Mazarakioti, S. Tzani, V. Psycharis, M. Pissas, Y. Sanakis, C. P. Raptopoulou, *Curr. Inorg. Chem.* 7 (2017) 66.
- [31] D. Dermitzaki, O. Bistola, M. Pissas, V. Psycharis, Y. Sanakis, C. P. Raptopoulou, *Polyhedron*, 2018, submitted.

- [32] Rigaku/MSM (2005). *CrystalClear*. Rigaku/MSM Inc., The Woodlands, Texas, USA.
- [33] (a) G. M. Sheldrick, *Acta Cryst.* A64 (2008) 112. (b) G. M. Sheldrick, *Acta Cryst.* C71 (2015) 3.
- [34] DIAMOND – Crystal and Molecular Structure Visualization, Ver. 3.1, Crystal Impact, Rathausgasse 30, 53111, Bonn, Germany.
- [35] G. B. Deacon, R. J. Phillips, *Coord. Chem. Rev.* 33 (1980) 227.
- [36] J.-F. Dong, L.-Z. Li, H.-Y. Xu, D.-Q. Wang, *Acta Crystallogr.* E63 (2007) m2300.
- [37] M. Dey, C. P. Rao, P. K. Saarenketo, K. Rissanen, *Inorg. Chem. Commun.* 5 (2002) 380.
- [38] S. K. Wolff, D. J. Grimwood, J. J. McKinnon, M. J. Turner, D. Jayatilaka, M. A. Spackman, *CrystalExplorer.3*, The University of Western Australia, Crawley, Australia, **2012**.
- [39] K. Takahashi, N. Hoshino, T. Takeda, S. Noro, T. Nakamura, S. Takeda and T. Akutagawa, *Inorg. Chem.* 54 (2015) 9423.
- [40] A. Bondi, *J. Phys. Chem.* 68 (1964) 441.
- [41] J. J. McKinnon, M. A. Spackman, A. S. Mitchell, *Acta Cryst.* B60 (2004) 627.

Table of Contents

Supramolecular networks based on hydrogen bonded cubane and dinuclear copper(II)-Schiff base complexes are discussed. The ligands adopt five different coordination modes and two protonation states. The lattice structures of the 3D networks are studied with Hirshfeld Surface analysis method.

ACCEPTED MANUSCRIPT

